

CEDARVILLE UNIVERSITY

A MULTI-INPUT MULTI-OUTPUT CONTROL MODEL FOR A HYDROFOIL BOAT WITH DIFFERENTIAL FRONT & REAR STRUT STEERING AND ACTUATED-WING-INDUCED ROLL

AUTHOR

JASON PAULUS

Address: 759 TAMARRON DRIVE
COLORADO SPRINGS, CO 80919

Phone: 719.466.9778

Email: JASONPAULUS130@CEDARVILLE.EDU

ADVISOR

DR. TIMOTHY DEWHURST

Address: 251 NORTH MAIN STREET
CEDARVILLE, OH 45314

Phone: 937.766.7654

Email: DEWHURST@CEDARVILLE.EDU

30 JUNE 2021



A Multi-Input Multi-Output Control Model for a Hydrofoil Boat with Differential Front & Rear Strut Steering and Actuated-Wing-Induced Roll

Jason M. Paulus

Cedarville University — Mechanical Engineering
jasonpaulus130@cedarville.edu

30 June 2021

A single-strut hydrofoil boat is a craft with two inline struts protruding from the ventral hull along the keel of the boat which have hydrofoil wings at their lower ends. Lateral stability of such a craft is conventionally achieved by turning of the front strut, with the rudder-like control input on the boat inducing a rolling and yawing moment that allows for the boat to be controlled like a bicycle. The Cedarville University Solar Boat team has been researching advancements to this single-strut hydrofoil boat design with the addition of differential front- and rear-strut rudder control, vectored thrust, and independently actuated side wings. Using aircraft flight dynamics principles and state-space control theory, a model of the Cedarville University solar boat was developed in order to achieve improved handling through tuned, automatic feedback-control of the flight control surfaces.

Nomenclature

$C_{\mathcal{L}\alpha}$	Lift coefficient slope	deg ⁻¹
$C_{\mathcal{L}0}$	Reference lift coefficient	-
$C_{\mathcal{L}}$	Lift coefficient	-
\mathbf{I}_n	Identity matrix of size n	-
I_{xx}	Moment of inertia about x -axis	kg·m ²
I_{xz}	Product of inertia about xz -plane	kg·m ²
I_{yy}	Moment of inertia about y -axis	kg·m ²
I_{zz}	Moment of inertia about z -axis	kg·m ²
K	Empirical factor	-
L	Roll axis moment	N·m
M	Pitch axis moment	N·m
N	Yaw axis moment	N·m
Q	Dynamic pressure	Pa
S_{sf}	Front strut submerged area	m ²
S_{sr}	Rear strut submerged area	m ²
S_w	Wing total surface area	m ²
V	Longitudinal velocity	m·s ⁻¹
X	Longitudinal body force	N
Y	Lateral body force	N
Z	Vertical body force	N

b_w	Wingspan	m
dx_{sf}	Longitudinal dist. COM to front strut COP	m
dx_{sr}	Longitudinal dist. COM to rear strut COP	m
dz_{fly}	Vertical distance COM to ideal waterline	m
dz_s	Vertical distance COM to strut end	m
m	Boat total mass	kg
p	Body frame roll rate	deg·s ⁻¹
q	Body frame pitch rate	deg·s ⁻¹
r	Body frame yaw rate	deg·s ⁻¹
u	Longitudinal velocity in body frame	m·s ⁻¹
v	Lateral velocity in body frame	m·s ⁻¹
w	Vertical velocity in body frame	m·s ⁻¹
\bar{y}	Spanwise location of wing centroid	m
y_1	Distance to aileron inboard edge	m
y_2	Distance to aileron outboard edge	m
α	Angle of attack	deg
α_0	Zero-lift axis	deg
γ_f	Front strut steering angle	deg
γ_r	Rear strut steering angle	deg
δ_a	Aileron deflection	deg
η	Factor for estimate of K value	-
θ	Pitch angle	deg
ρ	Fluid density	kg·m ⁻³
τ	Flap effectiveness parameter	-
ϕ	Roll angle	deg
ψ	Yaw angle	deg

Note: COM stands for center of mass and COP stands for center of pressure.

1 Introduction

The Cedarville University Solar Boat team has been a high-caliber competitor in the international Solar Splash competition hosted in the United States of America. This competition involves the creation of solar-powered electric boats optimized to convert solar energy into mechanical power as efficiently as possible to win competitive races. The team also has competed twice in the Dutch Solar Chal-

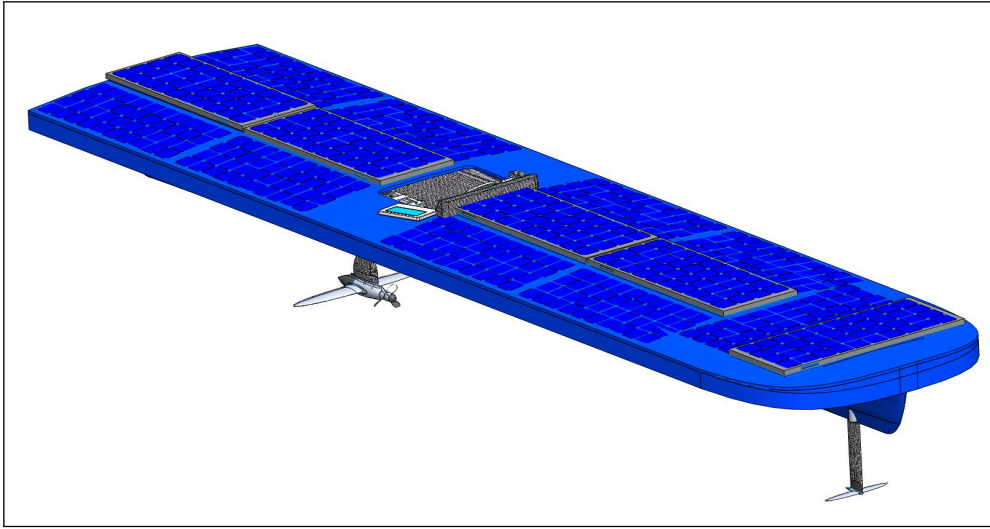


Fig. 1. CAD model of the Cedarville University hydrofoil solar boat

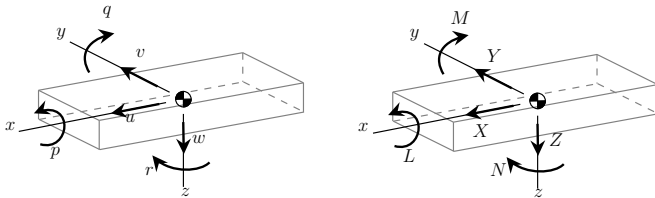


Fig. 2. Simplified kinematic diagram (left) & kinetic diagram (right) with axis convention (x, y, z) , body forces (X, Y, Z) , moments (L, M, N) , linear velocities (u, v, w) , and angular rates (p, q, r) .

lence in the Netherlands, but has not returned to compete since 2012. During this time, numerous senior-student design teams have been working on a twin-strut single-track hydrofoil boat in hopes of returning to the Netherlands and being a top competitor.

A large challenge that has faced the development of this new boat has been the creation and implementation of automatic fly-by-wire flight control software to allow the boat to fly on its hydrofoils to achieve minimal drag and therefore higher efficiency and performance. Competitors on the solar boat team of TU Delft have published [1] experimental validation for a state-space mathematical model of a single-track hydrofoil boat with manual control. In this paper, we will attempt to further develop this model to incorporate front-strut steering, rear-strut steering, and differentially-actuated wing control in a multi-input multi-output automatic feedback control loop to eventually be modified into an automatic flight control algorithm for the Cedarville hydrofoil boat.

2 DYNAMICAL MODEL OF A SINGLE-TRACK HYDROFOIL BOAT

For a dynamically moving craft, positions, velocities, and accelerations can be described either in a reference frame attached to the craft's body or in an inertial reference frame attached to, for example, the Earth. The conventions and nomenclature for a body reference frame are shown in the

kinematic and kinetic diagrams in Fig. 2. Following the axis convention used for aircraft, the x -axis is aligned with the longitudinal axis towards the front of the craft, the y -axis points laterally starboard, and the z -axis points ventrally.

2.1 Attitude equations

The orientation of an aircraft body is typically described with the Euler angles of roll (ϕ) , pitch (θ) , and yaw (ψ) . With an established body-frame coordinate system as shown in Fig. 3, transformation from the inertial frame to the body frame requires three transformations. The frame is first rotated about the inertial frame z -axis to give the craft's yaw in the "vehicle 1" frame, then rotated about the new y -axis to give pitch in the "vehicle 2" frame, and finally rotated about the vehicle-2 x -axis to give the roll of the body. These three respective transformations can be expressed by single-axis intrinsic rotation matrices:

$$R_I^{v1}(\psi) = \begin{bmatrix} \cos \psi & \sin \psi & 0 \\ -\sin \psi & \cos \psi & 0 \\ 0 & 0 & 1 \end{bmatrix} \quad (1)$$

$$R_{v1}^{v2}(\theta) = \begin{bmatrix} \cos \theta & 0 & \sin \theta \\ 0 & 1 & 0 \\ -\sin \theta & 0 & \cos \theta \end{bmatrix} \quad (2)$$

$$R_{v2}^b(\phi) = \begin{bmatrix} 1 & 0 & 0 \\ 0 & \cos \phi & -\sin \phi \\ 0 & \sin \phi & \cos \phi \end{bmatrix} \quad (3)$$

The resulting rotation matrix R to transform an arbitrary position vector $\mathbf{r}_I = [r_x, r_y, r_z]^T$ in the inertial frame to the body frame is:

$$\mathbf{r}_b = R_I^{v1}(\psi) R_{v1}^{v2}(\theta) R_{v2}^b(\phi) \mathbf{r}_I \quad (4)$$

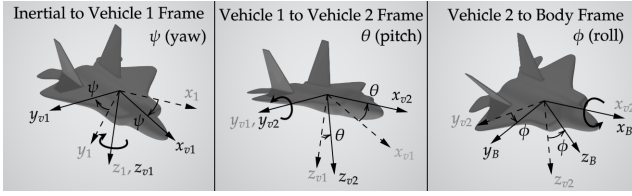


Fig. 3. Euler angle rotations. Yaw from inertial frame to Vehicle-1 Frame (left), pitch from Vehicle-1 frame to Vehicle-2 frame (middle), roll from Vehicle-2 frame to body frame (right)

2.2 Translational motion equations

Newton's second law of motion, expressed in the body frame, is:

$$m \frac{d\mathbf{V}_{CM}}{dt} \Big|_I = \mathbf{F}_b \quad (5)$$

where:

- $\frac{d\mathbf{V}_{CM}}{dt} \Big|_b$ is the acceleration of the boat expressed in the body reference frame,
- m is the mass of the boat, and
- \mathbf{F}_b is the external body forces on the boat, expressed in the body frame.

These forces include the hydrodynamic forces as well as the force of gravity.

$$\mathbf{F}_b = mg \begin{bmatrix} \sin \theta \\ \sin \phi \cos \theta \\ \cos \phi \cos \theta \end{bmatrix} + \begin{bmatrix} X \\ Y \\ Z \end{bmatrix} \quad (6)$$

Since the boat is taken to be rotating, the boat's acceleration in the inertial frame can be expressed by:

$$\frac{d\mathbf{V}_{cm}}{dt} \Big|_b = \frac{d\mathbf{V}_{cm}}{dt} \Big|_I + \boldsymbol{\omega}_b \times \mathbf{V}_{CM} \quad (7)$$

where:

- $\frac{d\mathbf{V}_{cm}}{dt} \Big|_I = [\dot{u}, \dot{v}, \dot{w}]^T$, the time rate of change of the boat velocity in the body frame,
- $\boldsymbol{\omega}_b = [p, q, r]^T$, the rotation rate vector components in the body frame, and
- $\mathbf{V}_{CM} = [u, v, w]^T$, the boat velocity components in the body frame, with no water current.

From Eqs. (6) and (7), Eq. (5) becomes:

$$m \begin{bmatrix} \dot{u} + qw - rv \\ \dot{v} + ru - pw \\ \dot{w} + pv - qu \end{bmatrix} = mg \begin{bmatrix} \sin \theta \\ \sin \phi \cos \theta \\ \cos \phi \cos \theta \end{bmatrix} + \begin{bmatrix} X \\ Y \\ Z \end{bmatrix} \quad (8)$$

2.3 Rotational motion equations

From the transport theorem in analytical dynamics, the time rate of change in an object's angular momentum \mathbf{L} in

a rotating frame is equal to the sum of external moments on the center of mass \mathbf{M}_{CM} which is expressed by:

$$\frac{d\mathbf{L}}{dt} = \mathbf{M}_{CM} = (\boldsymbol{\omega}_b \times I \boldsymbol{\omega}_b) + I \dot{\boldsymbol{\omega}}_b \quad (9)$$

where:

- $I = \begin{bmatrix} I_{xx} & -I_{xy} & -I_{xz} \\ -I_{xy} & I_{yy} & -I_{yz} \\ -I_{xz} & -I_{yz} & I_{zz} \end{bmatrix}$, the mass moment of inertia tensor,
- $\mathbf{M}_{CM} = [L, M, N]^T$, the external moments acting upon the craft, expressed in the body frame, and
- $\dot{\boldsymbol{\omega}}_b = [\dot{p}, \dot{q}, \dot{r}]^T$, the angular acceleration vector components in the body frame.

Since the angular acceleration components are of interest, we solve for the time rate of angular velocity, $\dot{\boldsymbol{\omega}}_b$:

$$\dot{\boldsymbol{\omega}}_b = I^{-1} (\mathbf{M}_{CM} - \boldsymbol{\omega}_b \times I \boldsymbol{\omega}_b) \quad (10)$$

which, with substitution, yields:

$$\begin{bmatrix} \dot{p} \\ \dot{q} \\ \dot{r} \end{bmatrix} = I^{-1} \left(\begin{bmatrix} L \\ M \\ N \end{bmatrix} - \begin{bmatrix} p \\ q \\ r \end{bmatrix} \times I \begin{bmatrix} p \\ q \\ r \end{bmatrix} \right) \quad (11)$$

The angular velocity vector in the body frame can be found from the time rates of change of the Euler angles in the inertial frame by:

$$\boldsymbol{\omega}_b = \begin{bmatrix} \dot{\phi} \\ 0 \\ 0 \end{bmatrix} + R_{v1}^b(\phi) \begin{bmatrix} 0 \\ \dot{\theta} \\ 0 \end{bmatrix} + R_{v1}^b(\phi) R_{v1}^{v2}(\theta) \begin{bmatrix} 0 \\ 0 \\ \dot{\psi} \end{bmatrix} \quad (12)$$

$$\begin{bmatrix} p \\ q \\ r \end{bmatrix} = \begin{bmatrix} 1 & 0 & -\sin \theta \\ 0 & \cos \theta & \sin \phi \cos \theta \\ 0 & -\sin \phi & \cos \phi \cos \theta \end{bmatrix} \begin{bmatrix} \dot{\phi} \\ \dot{\theta} \\ \dot{\psi} \end{bmatrix}$$

Inverting this equation yields:

$$\begin{bmatrix} \dot{\phi} \\ \dot{\theta} \\ \dot{\psi} \end{bmatrix} = \begin{bmatrix} 1 & \sin \phi \tan \theta & \cos \phi \tan \theta \\ 0 & \cos \phi & -\sin \phi \\ 0 & \sin \phi \sec \theta & \cos \phi \sec \theta \end{bmatrix} \begin{bmatrix} p \\ q \\ r \end{bmatrix} \quad (13)$$

2.4 Model simplifying assumptions

We now make several assumptions to simplify the model.

- Forward speed is a constant greater than zero, meaning the sum of forces in the longitudinal direction is zero ($X = 0$), the thrust force is equivalent to the drag on the boat ($F_T = D$), and longitudinal acceleration is zero ($\dot{u} = 0$).
- The model is linearized about a point where there is no sideslip or sideforce, hence $v_0 = 0$, $\dot{v} = 0$, $Y = 0$, $\dot{Y} = 0$.

- The model is linearized where the boat has no rotational rate or acceleration: $r_0 = 0, \dot{r}_0 = 0, \psi_0 = \phi_0 = 0, \dot{\psi}_0 = \dot{\phi}_0 = p_0 = 0, \dot{p}_0 = 0$.
- The boat maintains perfect longitudinal control such that there is no change in pitch ($\theta = 0, \dot{\theta} = q = 0, \dot{q} = 0, M = 0$) and the vertical forces sum to zero with no heaving motion ($Z = 0, \dot{Z} = 0, w = 0, \dot{w} = 0$).
- All surfaces operate in a region where the lift coefficient slope is linear.
- Rotation of the wings as a result of strut deflection γ is ignored.
- The boat is perfectly rigid with constant mass and mass distribution, and is symmetric about the xz plane: $I_{xy} = I_{yz} = 0$.
- The lift coefficients of the wing and struts are independent of Reynolds' number.
- The boat operates in a region of low roll ($<30^\circ$) so we can apply small angle assumption: $\sin \phi \approx \phi, \cos \phi \approx 1$.
- The propeller wash does not influence the flow field over the rear wings.

When we apply these assumptions to the translation, rotation, and attitude equations, the model is reduced to:

$$m \begin{bmatrix} -rv \\ \dot{v} + ru \\ pu \end{bmatrix} = \begin{bmatrix} 0 \\ mg\phi + Y \\ mg \end{bmatrix} \quad (14)$$

$$\begin{bmatrix} I_{xx}\dot{p} - I_{xz}\dot{r} \\ 0 \\ -I_{xz}\dot{p} + I_{zz}\dot{r} \end{bmatrix} = \begin{bmatrix} L \\ p(I_{zz}r - I_{xz}p) + r(I_{xx}p - I_{xz}r) \\ N \end{bmatrix} \quad (15)$$

$$\begin{bmatrix} \dot{\phi} \\ 0 \\ \dot{\psi} \end{bmatrix} = \begin{bmatrix} p \\ 0 \\ r \end{bmatrix} \quad (16)$$

It can be seen that there are only four unique variables describing the state of the boat: sideslip velocity v , roll angle ϕ , roll rate p , and yaw rate r . All the other terms are either parameters of the model (e.g. m), rates of these state variables (e.g. \dot{v}), or functions of them (e.g. L, N).

2.5 Single-rudder hydrofoil boat linear time-invariant model

Methods of modern control theory have been widely used to describe the dynamics of aircraft motion. To make use of these methods, we must transform our equations of motion into a continuous linear time-invariant (LTI) state-space form:

$$\dot{\mathbf{x}}(t) = \mathbf{A} \mathbf{x}(t) + \mathbf{B} \mathbf{u}(t) \quad (17)$$

$$\mathbf{y}(t) = \mathbf{C} \mathbf{x}(t) \quad (18)$$

where:

- $\mathbf{x}(t) = [v, \phi, p, r]^T$, the state vector,
- $\mathbf{u}(t)$ is the input vector,

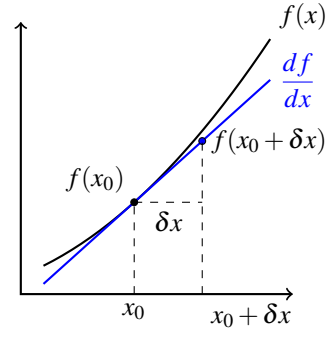


Fig. 4. Linearization of a nonlinear function

- $\mathbf{y}(t)$ is the output vector,
- \mathbf{A} is the state matrix,
- \mathbf{B} is the input matrix, and
- \mathbf{C} is the output matrix.

For the purposes of the front/rear steering model, we will consider the effect of one of the steering struts as the only input to the system. When either of the struts is turned by an angle γ , this changes its angle of attack and generates sideways lift on the strut, influencing the motion of the boat. Therefore, we define $\mathbf{u}(t) = \gamma(t)$. To prevent confusion with notation, forward velocity will hereafter be denoted by V .

To begin acquiring our state-space model, we start by solving our previously obtained equations for the highest-order derivatives. Two of these are already in the proper form in Eq. (16), the latter of which is not immediately relevant to our model. From Eq. (14), we can obtain:

$$\dot{v} = \frac{1}{m}Y + \frac{1}{m}mg\phi - rV \quad (19)$$

We can see that this equation is linear with respect to ϕ and V , but Y is a function of the state variables and must be linearized.

Linearization is the process of finding the linear approximation to a function at a given point, which is the first order Taylor expansion around the point of interest. From Fig. 4 it can be seen that close to some x_0 , the nonlinear function f can be approximated with a linear function, but only in a region local to the linearization point. In mathematical terms:

$$f(x) \approx f(x_0) + \delta x \left. \frac{df}{dx} \right|_{x_0} \quad (20)$$

For functions of multiple variables, it is the same idea:

$$f(\mathbf{x}) \approx f(\mathbf{x}_0) + \delta \mathbf{x} \cdot \nabla f \Big|_{\mathbf{x}_0} \quad (21)$$

which can be rearranged to express a relative change in the function value from the equilibrium point, rather than its ab-

solute value:

$$\Delta f \approx \delta \mathbf{x} \cdot \nabla f \Big|_{\mathbf{x}_0} \quad (22)$$

Applying this to Eq. (19) yields:

$$\Delta \dot{v} = \frac{1}{m} [Y_v \delta v + Y_\phi \delta \phi + Y_p \delta p + Y_r \delta r + Y_\gamma \delta \gamma] - V \delta r \quad (23)$$

The notation for linearized derivatives is introduced at this point — for example, $dY/dv \equiv Y_v$. It should also be noted that from Eq. (14) that in static equilibrium, $Y = mg\phi$ and so $Y_\phi = mg$, accounting for the second term in Eq. (19). The above equation can be rewritten as:

$$\dot{v} = \begin{bmatrix} Y_v/m & Y_\phi/m & Y_p/m & Y_r/m & -V \end{bmatrix} \mathbf{x} + \begin{bmatrix} Y_\gamma/m \end{bmatrix} \mathbf{u} \quad (24)$$

From Eq. (15), the rate terms can be solved for as:

$$\dot{p} = LK_{zz} + NK_{xz} \quad (25)$$

$$\dot{r} = LK_{xz} + NK_{xx} \quad (26)$$

where:

$$\begin{aligned} \square K_{xx} &= \frac{I_{xx}}{I_{xx}I_{zz} - I_{xz}^2} \\ \square K_{zz} &= \frac{I_{zz}}{I_{xx}I_{zz} - I_{xz}^2} \\ \square K_{xz} &= \frac{I_{xz}}{I_{xx}I_{zz} - I_{xz}^2} \end{aligned}$$

Linearizing yields:

$$\dot{p} = [L_v K_{zz} + N_v K_{xz}, \quad L_\phi K_{zz} + N_\phi K_{xz}, \quad L_p K_{zz} + N_p K_{xz}, \quad L_r K_{zz} + N_r K_{xz}] \mathbf{x} + [L_\gamma K_{zz} + N_\gamma K_{xz}] \mathbf{u} \quad (27)$$

$$\dot{r} = [L_v K_{xz} + N_v K_{xx}, \quad L_\phi K_{xz} + N_\phi K_{xx}, \quad L_p K_{xz} + N_p K_{xx}, \quad L_r K_{xz} + N_r K_{xx}] \mathbf{x} + [L_\gamma K_{xz} + N_\gamma K_{xx}] \mathbf{u} \quad (28)$$

The assumption that ϕ only affects the gravitic vector means that the partials with respect to ϕ go to 0. The result of these linearized equations is the complete state-space model, where:

$$\mathbf{A} = \begin{bmatrix} Y_v/m & Y_\phi/m & Y_p/m & Y_r/m - V \\ 0 & 0 & 1 & 0 \\ L_v K_{zz} + N_v K_{xz} & 0 & L_p K_{zz} + N_p K_{xz} & L_r K_{zz} + N_r K_{xz} \\ L_v K_{xz} + N_v K_{xx} & 0 & L_p K_{xz} + N_p K_{xx} & L_r K_{xz} + N_r K_{xx} \end{bmatrix} \quad (29)$$

$$\mathbf{B} = \begin{bmatrix} Y_\gamma/m \\ 0 \\ L_\gamma K_{zz} + N_\gamma K_{xz} \\ L_\gamma K_{xz} + N_\gamma K_{xx} \end{bmatrix} \quad (30)$$

The output matrix \mathbf{C} is the identity matrix. This choice is not unique, but it is useful to output all of the states when the model is run with a program such as MATLAB or Simulink.

3 COMPARISON OF FRONT AND REAR-STEERING MODELS

In the model derived in the previous section, the input is a generic rudder deflection γ . This can represent either front or rear-rudder steering, depending on the definition of the input derivatives (Y_γ , L_γ , & N_γ) in Eq. (30).

3.1 Front steering input derivatives

For a deflection of the front steering strut measured by angle γ_f , the angle of attack of the strut foil is given by $\alpha = \gamma_f$. The steering angle is defined such that positive strut deflection creates a positive sideforce, and thus the strut turns to the right from the pilot's perspective. While operating in the linear region of the strut's lift coefficient slope, the sideforce created on the strut is:

$$Y = \frac{1}{2} \rho V^2 S_{sf} C_{\mathcal{L}\alpha s} \gamma_f \quad (31)$$

where $C_{\mathcal{L}\alpha s}$ is the lift coefficient slope of the strut. This force acts at the vertical center of pressure of the submerged area of the strut and creates a negative moment about the roll axis:

$$L = -Y \left(\frac{dz_s + dz_{fly}}{2} \right) \quad (32)$$

as well as a positive yawing moment based on the strut's distance from the center of mass:

$$N = Y \cdot dx_{sf} \quad (33)$$

It can be easily seen that the derivative of sideforce with respect to front steering angle is:

$$Y_{\gamma_f} = \frac{1}{2} \rho V^2 S_{sf} C_{\mathcal{L}\alpha s} \quad (34)$$

and the derivatives L_{γ_f} and N_{γ_f} follow suit. For brevity, these terms are listed in Table 1.

3.2 Rear steering input derivatives

For a deflection of the rear steering strut measured by angle γ_r , the angle of attack of the strut foil is given by $\alpha = \gamma_r$, once again defined such that a positive turn creates positive sideforce. A significant difference between the rear-steering and front-steering models is the propeller at the end of the rear strut, shown in Fig. 1. The propeller is assumed to generate a constant thrust force F_T in-line with the angle of the strut and hub assembly. Using the small angle assumption, the lateral component of this thrust force can be expressed by $F_T \gamma_r$ and the total sideforce generated is:

$$Y = \frac{1}{2} \rho V^2 S_{sr} C_{\mathcal{L}\alpha s} \gamma_r + F_T \gamma_r \quad (35)$$

Table 1. Summary of front and rear steering derivatives

Front steering	Rear steering
$Y_{\gamma_f} = \frac{1}{2}\rho V^2 S_{sf} C_{\mathcal{L}\alpha_s}$	$Y_{\gamma_r} = \frac{1}{2}\rho V^2 S_{sr} C_{\mathcal{L}\alpha_s} + F_T$
$L_{\gamma_f} = -\frac{1}{2}\rho V^2 S_{sf} C_{\mathcal{L}\alpha_s} \left(\frac{dz_s + dz_{fly}}{2} \right)$	$L_{\gamma_r} = -\frac{1}{2}\rho V^2 S_{sr} C_{\mathcal{L}\alpha_s} \left(\frac{dz_s + dz_{fly}}{2} \right) - F_T \cdot dz_s$
$N_{\gamma_f} = \frac{1}{2}\rho V^2 S_{sf} C_{\mathcal{L}\alpha_s} \cdot dx_{sf}$	$N_{\gamma_r} = -\left(\frac{1}{2}\rho V^2 S_{sr} C_{\mathcal{L}\alpha_s} + F_T \right) dx_{sr}$

Both components of this force generate a negative roll moment, as with front-steering, but the propeller's thrust is generated at the end of the strut rather than at the center of pressure:

$$L = -Y \left(\frac{dz_s + dz_{fly}}{2} \right) - F_T \gamma_r \cdot dz_s \quad (36)$$

The yawing moment, however, is negative due to the force being opposite the COM compared to the front-steering model. The thrust force is assumed to cross through the centerline of the boat at the rear strut pivot axis, giving it the same yaw moment arm as the hydrodynamic lift force:

$$N = -(Y + F_T \gamma_r) dx_{sr} \quad (37)$$

Once again, the derivatives of these terms follow easily:

$$Y_{\gamma_r} = \frac{1}{2}\rho V^2 S_{sr} C_{\mathcal{L}\alpha_s} + F_T \quad (38)$$

and so forth. The terms can be seen in Table 1.

4 FEEDBACK-CONTROLLED NUMERICAL SIMULATION MODEL

4.1 Reasoning

In van Marrewijk [1], the TU Delft Solar Boat team used their single-track hydrofoil boat to experimentally validate the front-steering model presented here. Their methodology involved acquiring real-time measurements of the state and input variables during operation of the boat on water, and then comparing the boat state data with the response of the model to the same input variable data. Our goal was to also gather data with flight control tests, but the Cedarville University hydrofoil boat was being rebuilt during the extent of this work, so we were forced to take a theoretical approach.

The steering response tests by van Marrewijk were performed at approximately 0.47 Hz and 2.50 Hz steering input frequencies [1]. In the initial stages of theory development, when we input sine inputs of these frequencies to the state-space model, we found that the response was unstable and deviated towards infinity. The reason for this is because the model *is* inherently unstable. Since the TU Delft solar

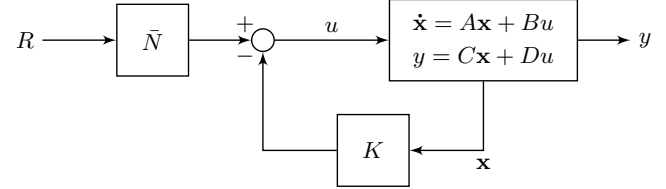


Fig. 5. Block diagram representation of precompensated state-space feedback control loop. Adapted from “Control tutorials for MATLAB” [2]

boat has no lateral feedback control for steering, the boat is controlled like a bike, and thus it is similar in that constant micro-adjustments in steering are necessary to maintain balance. Simple sine wave input does not account for this, resulting in the unstable behavior of the model. This posed a further challenge to our progress.

Our solution was to mathematically derive a feedback-controlled simulation model, which can be represented by the block diagram in Fig. 5. With a mechanically linked steering wheel control, as on the TU Delft solar boat, the strut steering angle is directly proportional to the steering wheel input, so the input signal u is effectively γ . As discussed above, making this setup stable is only possible through manual control of the steering wheel. Since this was not possible for us, we used methods of modern control theory to create a stable feedback loop to allow us to examine the results of the front-steering and rear-steering models.

In the setup depicted in Fig. 5, the independently controlled variable is R , typically called the setpoint of the model. Rather than manually controlling the input u , the feedback loop reads the state \mathbf{x} of the boat and compares it to the desired state R , adjusting u accordingly. For our simulation setup, we chose yaw rate r to be the variable for the setpoint. The justification for this decision was that when the pilot turns the steering wheel, the *desired* command is not directly the strut angle but rather the turn rate, like what one would expect when turning the steering wheel of a car. Therefore, with feedback control as shown, the model will track the setpoint and remain stable, allowing us to examine its behavior. During simulation testing, the setpoint signal can be any value or data curve that we desire, and for physical implementation on the boat, the signal will come from a rotary encoder on the steering shaft that will relay the position of the steering wheel to the flight control system.

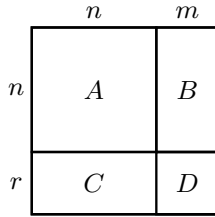


Fig. 6. The sizes of the state-space matrices must be as shown in the diagram, with n as the number of states, m as the number of inputs, and r as the number of outputs. Adapted from MathWorks [3]

4.2 Design methodology

The first step in this design is to choose a suitable feedback gain K that makes the closed-loop system stable. If the reference input is set to zero, then the input is $\mathbf{u} = -K\mathbf{x}$ and, with substitution into Eq. (17):

$$\dot{\mathbf{x}} = (\mathbf{A} - \mathbf{BK})\mathbf{x} \quad (39)$$

where the coefficient of \mathbf{x} is called the closed loop state matrix. The eigenvalues of this matrix are what determine the location of the closed loop poles, so (with an observable and controllable system) we can create an equation knowing our desired poles, \mathbf{P} , and choose K accordingly:

$$\text{eig}(\mathbf{A} - \mathbf{BK}) = \mathbf{P} \quad (40)$$

Jürgen Ackermann's formula [4] states that the process of choosing a suitable feedback gain can be simplified by only computing one equation:

$$K = [\underbrace{0 \ 0 \ \dots \ 0}_{n-1} \ 1] \mathcal{C}^{-1} p_{\text{new}}(\mathbf{A}) \quad (41)$$

where $p_{\text{new}}(\mathbf{A})$ is the desired closed-loop characteristic polynomial evaluated at the state matrix \mathbf{A} , n is the number of states, and \mathcal{C} is the controllability matrix of the system given by:

$$\mathcal{C} = [\mathbf{B} \ \mathbf{AB} \ \mathbf{A}^2\mathbf{B} \ \dots \ \mathbf{A}^{n-1}\mathbf{B}] \quad (42)$$

These equations can be performed in MATLAB with the `place()` or `acker()` built-in functions [5].

With K obtained, the feedback control model is now stable and returns to equilibrium from an initial disturbance. However, if the reference input is changed from zero, the respective output state will not necessarily settle at the value of R . A precompensation gain, \bar{N} , is necessary to scale the reference input to equal the feedback signal $K\mathbf{x}$ in steady state. The value of this gain can be found by:

$$\bar{N} = [K \ \mathbf{I}_m] \begin{bmatrix} \mathbf{A} & \mathbf{B} \\ \mathbf{C} & \mathbf{D} \end{bmatrix}^{-1} \begin{bmatrix} 0_n \\ \mathbf{I}_r \end{bmatrix} \quad (43)$$

where m is the number of inputs and r is the number of outputs as in Fig. 6 (both 1 in this case).

4.3 Testing and evaluation

The state-space matrices were calculated using the parameters for the TU Delft solar boat listed in van Marrewijk [1] — for which the front-steering state-space model was experimentally validated — with the addition of $F_T = 250$ N representing the approximate thrust necessary to overcome drag at 10 m/s. We found that pole locations of $-8 \pm 5i$, -34 , & -3400 gave desirable response characteristics for both the front and rear-steering models. The corresponding feedback and precompensation gains calculated using these poles and the state-space matrices from TU Delft's solar boat are listed in Table 2. Note that the scaling factor of $\pi/180$ converts a command value of deg/s to rad/s for calculation in the state-space model.

The matrices and gains were then implemented in a Simulink model for testing, which was beneficial for understanding dynamics of the boat. For instance, one lesson we learned was that the model behaved very poorly when subjected to a step input, with yaw rate spiking an order of magnitude larger than, and in the opposite direction of, the commanded yaw rate. Though this spike was less than 0.25 seconds in duration, and stabilized to the commanded value within 1 second, it still resulted in a significant adverse turn. However, since a step input is not realistic for the physical system, we ignored this issue and opted to use a sine-ramped step input which, when put into the Simulink program, caused favorable response of the models.

The example setpoint curve we chose instead is a two-second sine ramp up to 10 deg/s, held for four seconds, followed by a two-second sine ramp down, which we believed to be representative of a driver's input on a steering wheel during a turn. The integral of this desired yaw rate equals a 60° turn to the right that should be completed by the model. The curve and the responses of the front and rear-steering models to this setpoint curve are shown in Figs. 7 & 8.

An expected but nevertheless interesting phenomenon can be seen in the response of both models. When a positive yaw rate command is introduced, the control input generated to do so is initially (at approximately $t = 3$ s) opposite what should be necessary to make a positive turn. After stabilization, the same holds true again when the command is reversed at approximately $t = 9$ s. We explain this behavior as like riding a bicycle, where when one wants to turn to the right, they must first steer left to begin falling to the right, and then steer into that fall to make the turn. With a rear-steering model, the concept is paralleled but with the steering direction reversed. We predicted this behavior before the existence of these results, so it leads us to believe we are testing the model behavior in accurate and effective manner.

When the model behaviors are compared, it can be seen that the front steering model's yaw rate quickly tracks to the setpoint at steady state but has significant deviance to maintain stability and control when the setpoint is changing. The rear steering model, on the other hand, follows the shape of the setpoint curve more closely but with a significant lag. The front steering model's heading curve settles at the predicted 60° almost simultaneously with the flattening of the

Table 2. Computed values for feedback and precompensation gains used in front and rear steering simulation models

Steering	K	\bar{N}
Front	$[4.0325 \quad -196.9836 \quad -11.2395 \quad 0.7965]$	$-191.4162 \cdot \frac{\pi}{180}$
Rear	$[16.1330 \quad 234.9360 \quad -3.3098 \quad -5.5975]$	$187.4735 \cdot \frac{\pi}{180}$

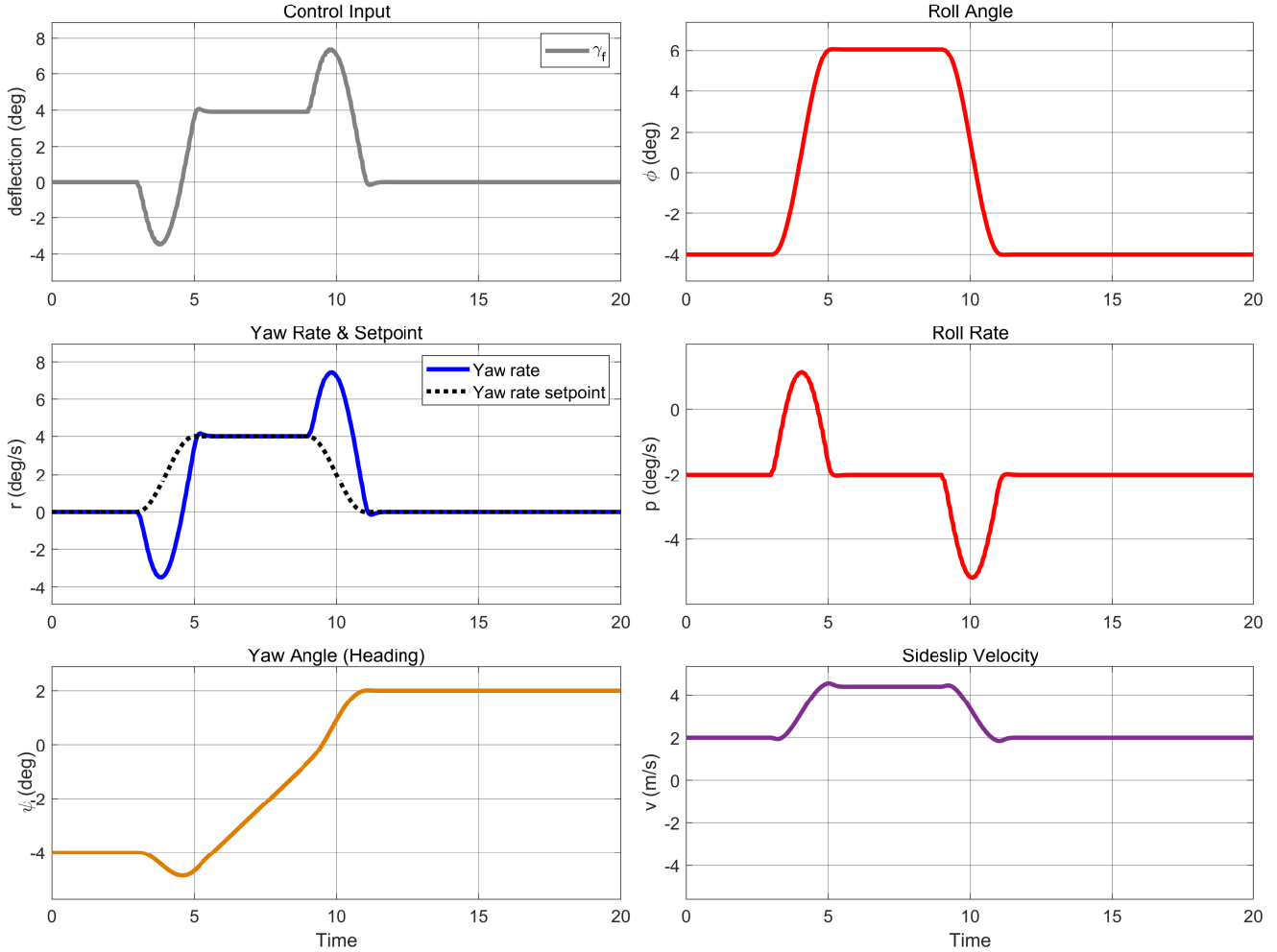


Fig. 7. Input and response curves for front steering model, acquired from Simulink simulated feedback control model. Yaw rate setpoint is a two-second sine-ramped step to 10 deg/s starting at $t = 3$ s, a four-second hold, and a two-second sine-ramped step down to 0 deg/s.

setpoint curve, while the rear steering model falls a few degrees short of the expected heading and settles nearly four seconds after the yaw command is flattened.

The sideslip velocity curves also reveal behaviors of the two models. With the front steering model, sideslip is positive and roughly proportional to the roll angle curve. This indicates that the boat is departing from coordinated flight and sliding laterally along the plane of the wings due to the influence of gravity. This is a well-known phenomenon in aircraft flight dynamics, and its presence in the response reinforces our confidence in the model’s behavior. The rear steering model achieves lateral velocity *away* from the direction of bank and turn, a motion which is typically referred to as skid. This can be attributed to the lateral contribution of the vectored thrust, as the sideslip curve is roughly propor-

tional to the control input curve.

Although the results are promising, the models are notably limited by the simplifying assumptions in the derivations. For instance, in Eq. (16) the small-angle assumption led to the result that $\dot{\phi} = r$. It’s intuitive to see that this holds for small angles of roll or pitch, but at higher angles this becomes inaccurate, and r cannot be used alone to get the true measure of the turn. If the craft is in a bank, then r (defined in the body frame) indicates that the craft is only rotating on the plane of the wings. If enough yaw in the body frame is achieved, this could lead to the nose pointing directly into the water. A form of pitch control would be necessary to maintain a level attitude when in a banked turn.

We furthermore surmise that the behavior of the rear steering model in particular deviates very quickly from the

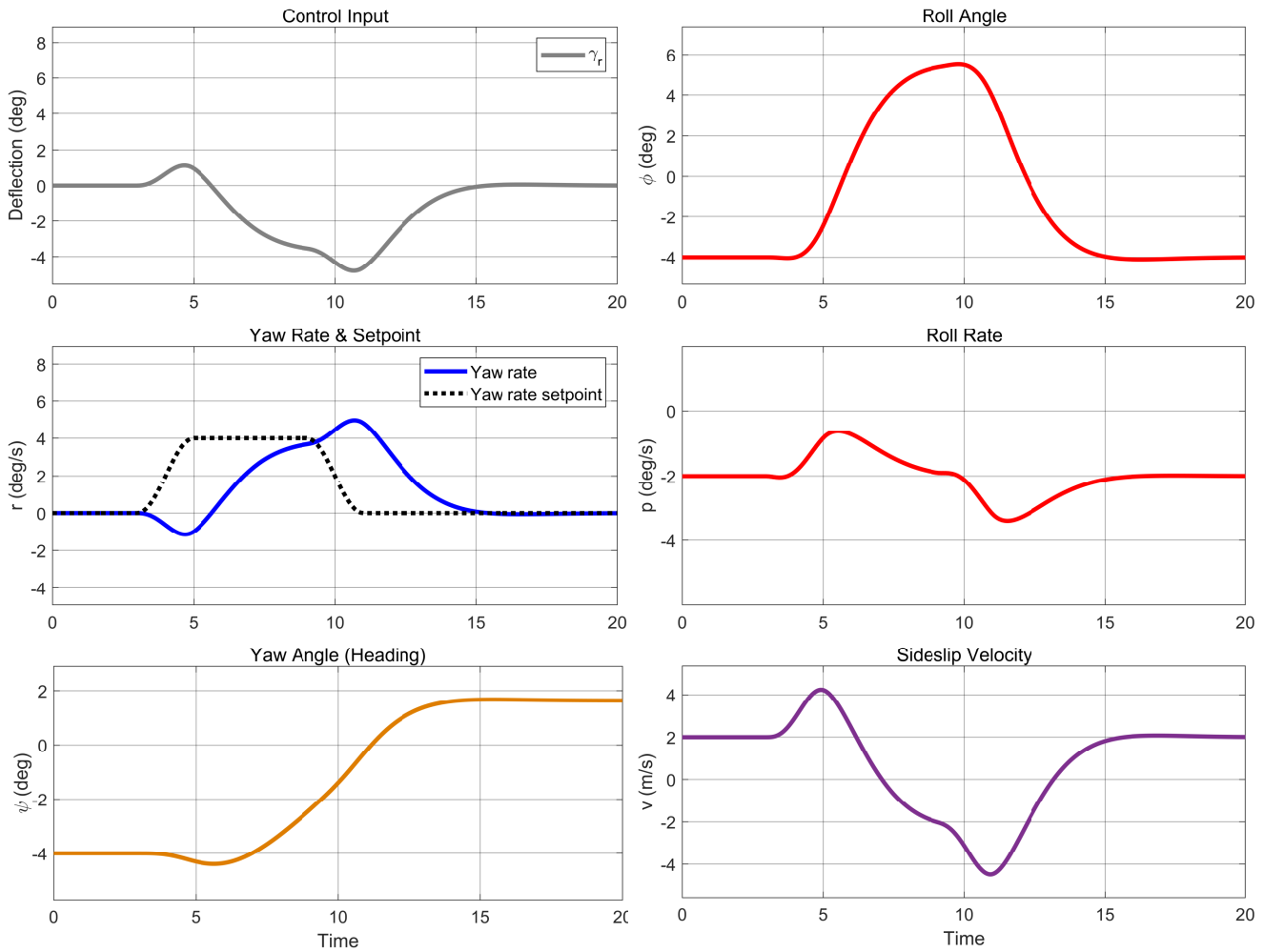


Fig. 8. Input and response curves for rear steering model, acquired from Simulink simulated feedback control model. Yaw rate setpoint is a two-second sine-ramped step to 10 deg/s starting at $t = 3$ s, a four-second hold, and a two-second sine-ramped step down to 0 deg/s.

linearity of the mathematical model due to the large additional force from the lateral component of thrust. Notice that when in a right-hand turn with positive roll, the rear strut is commanded to point left, or towards the surface. We believe that this could cause a tendency for the vectored thrust to wrest the aft of the boat towards the surface of the water and significantly change the dynamics of the turn. This should be addressed with a fully coupled lateral-longitudinal simulation model.

5 DERIVATION OF RUDDER & WINGERON MULTI-INPUT MULTI-OUTPUT MODEL

In contrast to the TU Delft solar boat, the Cedarville University hydrofoil boat has the capability to pivot both the front and rear struts independently, as well as the ability to differentially actuate its rear foils [6], allowing them to serve the same function as aileron control surfaces on an aircraft. The combination of the actuated wing input with strut steering in the state-space model allowed for the creation of a multi-input multi-output (MIMO) system with front-rudder (γ_f), rear-rudder (γ_r), and “aileron” (δ_a) inputs. Since each rear foil entirely serves the functions of both wing

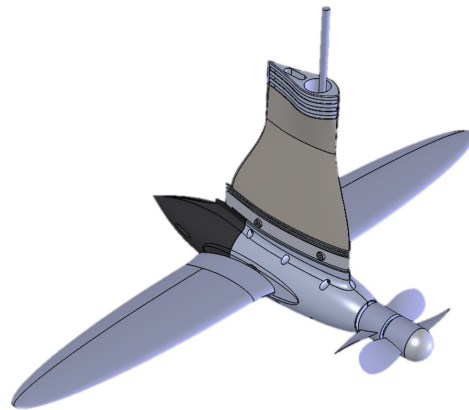


Fig. 9. CAD model of the CU hydrofoil boat rear strut assembly including the gearbox pod, propeller, and rear foils

and aileron, the typical term for the foil is called a wingeron (portmanteau of “wing-aileron”), which is how we will refer to it henceforth. To derive the model, we considered the process we took for derivation of the rear-steering model and started the same method, attempting to derive the input re-

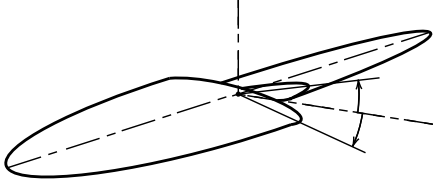


Fig. 10. Diagram of positive wingeron deflection

sponse from first principles. As this work progressed, we realized it was akin to a model developed by Nelson [7] for a lateral model of a fixed-wing aircraft with aileron and rudder input.

The introduction of the new inputs to the state-space boat model will not affect the state matrix \mathbf{A} , as the boat still responds identically to the states. The new inputs affect the input matrix \mathbf{B} , however, with new columns describing the boat's response to each separate input:

$$\mathbf{B} \mathbf{u} = \begin{bmatrix} Y_{\gamma_f}/m & Y_{\eta}/m & 0 \\ 0 & 0 & 0 \\ L_{\gamma_f}K_{zz} + N_{\gamma_f}K_{xz} & L_{\eta}K_{zz} + N_{\eta}K_{xz} & L_{\delta_a}K_{zz} + N_{\delta_a}K_{xz} \\ L_{\gamma_f}K_{xz} + N_{\gamma_f}K_{xx} & L_{\eta}K_{xz} + N_{\eta}K_{xx} & L_{\delta_a}K_{xz} + N_{\delta_a}K_{xx} \end{bmatrix} \begin{bmatrix} \gamma_f \\ \eta \\ \delta_a \end{bmatrix} \quad (44)$$

The primary things to note about this equation, aside from the new variable δ_a for “aileron” deflection, is the new derivatives L_{δ_a} & N_{δ_a} , and that the top rows are not similar. The latter is explained most easily, as it should be intuitively obvious to tell that wingeron deflection creates no side force and thus does not influence sideslip, so the matrix term on that row is zero. Rows three and four of the third column are similar to those of the first and second columns, so only the new terms L_{δ_a} & N_{δ_a} will be discussed. In these derivations, the subscript of w will be used for “wing,” which refers to the rear foils of the boat(s).

The change in aerodynamic yaw moment with respect to a change in aileron angle — an effect which is referred to as adverse yaw, as it opposes the direction of bank — is given [7] by:

$$N_{\delta_a} = \frac{QS_w b_w}{I_{zz}} C_{n_{\delta_a}} \quad (45)$$

where Q is dynamic pressure, S_w is the total planform surface area of both wings, b_w the wingspan, and $C_{n_{\delta_a}}$ is the change of the aerodynamic coefficient of yaw (C_n), with respect to aileron deflection. This derivative is given as:

$$C_{n_{\delta_a}} = 2KC_{\mathcal{L}_0}C_{l_{\delta_a}} \quad (46)$$

where K is an empirical constant, $C_{\mathcal{L}_0}$ is the reference lift coefficient, and $C_{l_{\delta_a}}$ is the control power of aileron deflection. The constant K is tabulated [7] as a function of an aileron factor η and wing aspect ratio AR as shown in Fig. 11. The aileron factor η is given as:

$$\eta = \frac{y_1}{b_w/2} \quad (47)$$

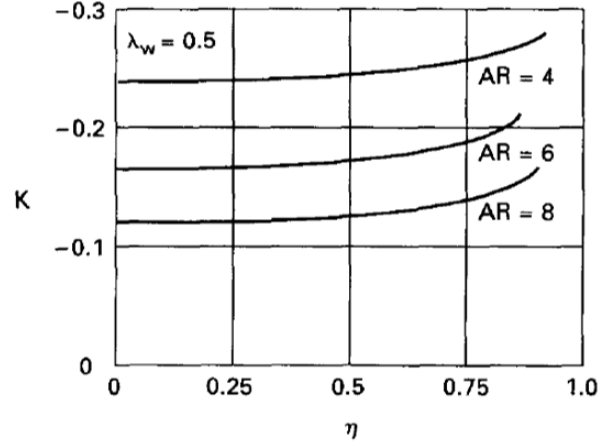


Fig. 11. Tabulated values for empirical constant K as a function of aileron factor η and aspect ratio AR . From Nelson, Flight Stability & Automatic Control, 2 ed.

where y_1 is the spanwise distance from the centerline to the aileron inboard edge, and $b_w/2$ is the semispan. Aspect ratio is defined as:

$$AR = \frac{b_w^2}{S_w} \quad (48)$$

The reference lift coefficient is defined as:

$$C_{\mathcal{L}_0} = C_{\mathcal{L}_\alpha} |\alpha_0| \quad (49)$$

where $C_{\mathcal{L}_\alpha}$ is the lift coefficient slope and α_0 is the zero-lift angle of attack. The control power of aileron deflection is given as:

$$C_{l_{\delta_a}} = \frac{2C_{\mathcal{L}_\alpha w} \tau}{S_w b_w} \int_{y_1}^{y_2} c(y) \cdot y \, dy \quad (50)$$

where τ is the flap effectiveness parameter (which can be approximated to 1 for a wingeron), $c(y)$ is the chord as a function of spanwise distance y , and y_1 & y_2 denote the spanwise distances of the inboard and outboard edges of the aileron. Since in our case the entire wing is the control surface, y_1 & y_2 indicate the wing root and tip respectively, and the integral in Eq. (50) can be thought of as the first moment of area of the wing. Since for a shape bounded by an arbitrary curve $g(x)$ and lines $x = x_1$, $x = x_2$, & $y = 0$ giving an area A , the centroid \bar{x} of the shape can be found by:

$$\bar{x} = \frac{1}{A} \int_{x_1}^{x_2} g(x) \cdot x \, dx \quad (51)$$

We note that the integral is the same form as the integral in Eq. (50), so solving for it yields:

$$\int_{x_1}^{x_2} g(x) \cdot x \, dx = \bar{x}A \quad (52)$$

and therefore, equivalently:

$$\int_{y_1}^{y_2} c(y) \cdot y \, dy = \bar{y} S_w \quad (53)$$

where \bar{y} is the spanwise centroid of the wing. Using an elliptical wing assumption, the centroid is taken as:

$$\bar{y} = \frac{4(b_w/2)}{3\pi} \quad (54)$$

With Eqs. (46) to (50), (53) and (54), Eq. (45) can be expressed by:

$$N_{\delta_a} = \frac{8K\tau Q S_w b_w (C_{\mathcal{L}_{\alpha w}})^2 \alpha_0}{3\pi I_{zz}} \quad (55)$$

noting that this is only applicable for an elliptical or near-elliptical wing. The second and last new stability derivative, L_{δ_a} , is given by:

$$\begin{aligned} L_{\delta_a} &= \frac{Q S_w b_w C_{l_{\delta_a}}}{I_{xx}} \\ &= \frac{8\tau Q S_w b_w C_{\mathcal{L}_{\alpha w}}}{3\pi I_{xx}} \end{aligned} \quad (56)$$

To implement these equations for the Delft boat, we needed a few extra parameters. First, the wing aspect ratio is:

$$AR = \frac{b_w^2}{S_w} = \frac{(0.997 \text{ m})^2}{(0.0681 \text{ m}^2)} = 14.6 \quad (57)$$

which is well off the tabulated range. The aileron factor η is approximated to be 0, due to actuation of the entire wing. We performed a Farazdaghi-Harris-model curve fit [8] of the three data points at $\eta = 0$, and approximated the value of K at the calculated aspect ratio to be -0.0583 .

Since we do not have information about the shape of the TU Delft boat's foils, we assumed an elliptical foil shape. The ellipse fitting the given constraints of wingspan and wing area has a root chord of 0.087 m which is less than the strut chord, which we believe justifies this assumption. Again, we do not have information on the foils to obtain the zero-lift angle of attack. Typical values for α_0 are between -0° and -15° , and for the MH115 foils on the CU solar boat the value is about -7° [6], so we use this value as an estimate of α_0 . The stability derivatives for the aileron deflection column of matrix \mathbf{B} can then be computed.

6 EVALUATION OF RUDDER & WINGERON MULTI-INPUT MULTI-OUTPUT MODEL

6.1 Design methodology

The design of a MIMO feedback control system incorporating front steering, rear steering, and wingeron action

follows the same procedure as in Section 4.2, but with a few details that should be noted. First, K must result in a 3×4 matrix in order to give a 3×1 feedback signal to the comparator. In MATLAB, the `place()` and `acker()` functions will automatically handle this based on the dimensions of \mathbf{B} .

$$\bar{N} = [K \ \mathbf{I}_m] \begin{bmatrix} \mathbf{A} & \mathbf{B} \\ \mathbf{C} & \mathbf{D} \end{bmatrix}^{-1} \begin{bmatrix} \mathbf{0}_n \\ \mathbf{I}_r \end{bmatrix} \quad (43)$$

Second, from Eq. (43) (reprinted above for convenience), we can see that the \mathbf{ABCD} matrix must be square in order to be inverted, meaning the output quantity r must equal the input quantity m . Even though we have four outputs, this is not an issue. In the state-space model we can still leave \mathbf{C} as it is, but we will modify it for calculating K in a way that “tells” the system which variables we want to control. Since we have three inputs to the model, this gives us the opportunity to govern three states with setpoints. In this situation, we desire to control sideslip velocity, roll, and body yaw rate — the first, second, and fourth states — so our modified \mathbf{C} becomes:

$$\mathbf{C} = \begin{bmatrix} 1 & 0 & 0 & 0 \\ 0 & 1 & 0 & 0 \\ 0 & 0 & 0 & 1 \end{bmatrix} \quad (58)$$

Lastly, the third term in the equation must have inverse dimensions of the first term, i.e. 6×3 . The identity matrix of size $r = 3$ fulfills the width criterion, and the rest of the digits are required to be zero, making:

$$\begin{bmatrix} \mathbf{0}_n \\ \mathbf{I}_r \end{bmatrix} = \begin{bmatrix} 0 & 0 & 0 \\ 0 & 0 & 0 \\ 0 & 0 & 0 \\ 0 & 0 & 0 \\ 1 & 0 & 0 \\ 0 & 1 & 0 \\ 0 & 0 & 1 \end{bmatrix} \quad (59)$$

Using the same pole locations as were used for the previous models, we calculate the feedback and precompensation gains in Table 3.

6.2 Testing and evaluation

We used the same experimental setup as in Section 4.3, setting the commanded roll rate magnitude in degrees to be equivalent to the yaw rate magnitude in degrees per second and using the same setpoint curve shape as used previously, with sideslip velocity commanded to 0 m/s. The results of a 20-second simulation are shown in Fig. 12.

Immediately noticeable is how well yaw rate and roll angle track with their setpoints compared to the single-input models in Figs. 7 and 8. When compared to the yaw rate response of the front-steering-only model in Fig. 7, it can

Table 3. Computed values for feedback and precompensation gains used in the wingeron MIMO model

K	\bar{N}
$\begin{bmatrix} 1.1833 & -11.1560 & -0.5730 & 24.8014 \\ -0.4076 & 9.3478 & 0.6683 & -21.9404 \\ 3.7121 & 39.6515 & 0.8311 & -96.3300 \end{bmatrix}$	$\begin{bmatrix} 1.3363 & -11.3034 & 25.1316 \\ -0.2617 & 9.2143 & -22.0057 \\ 4.5120 & 37.4332 & -95.1927 \end{bmatrix} \cdot \frac{\pi}{180}$

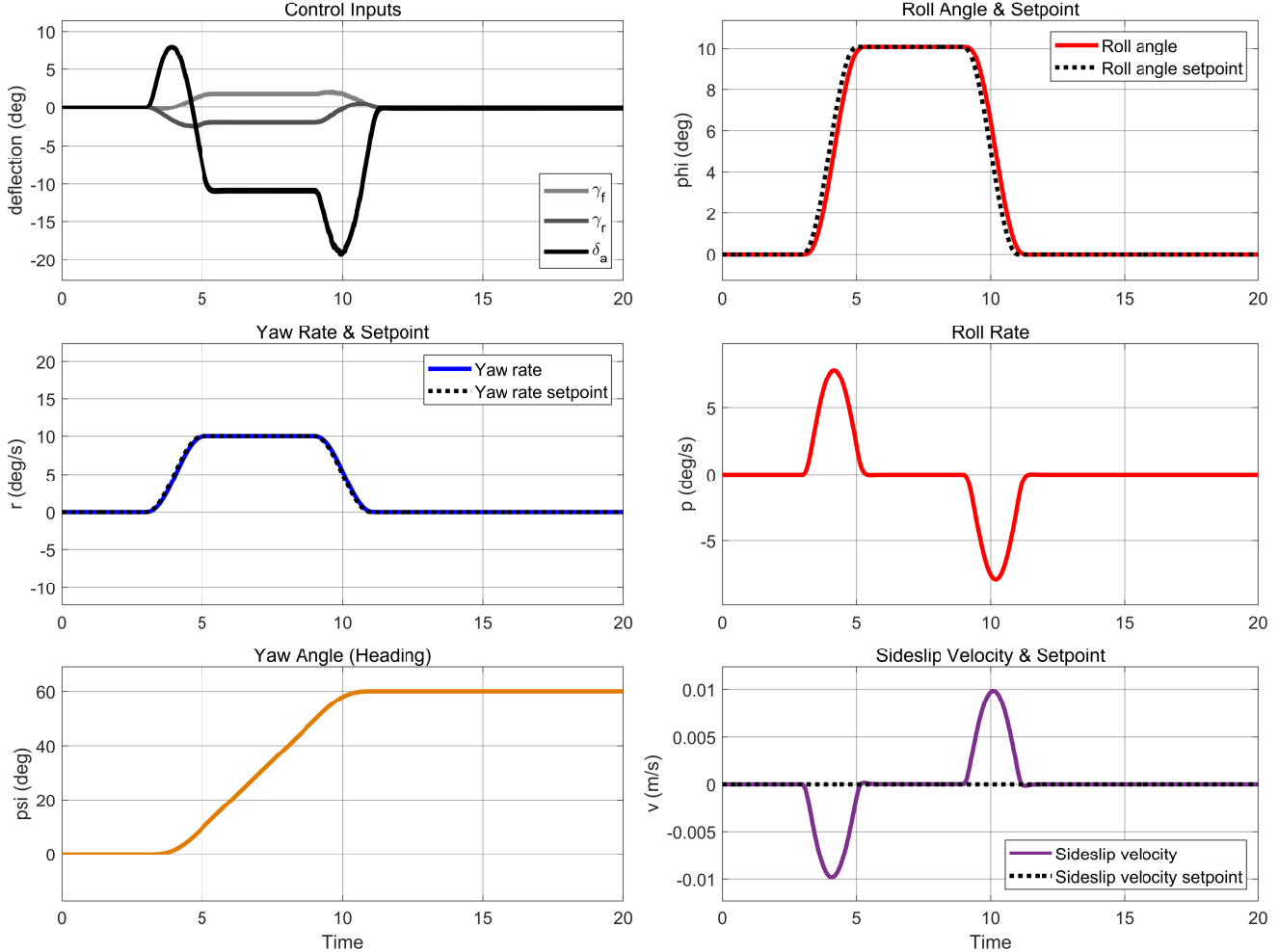


Fig. 12. Input and response curves for front steering - rear steering - wingeron MIMO model, acquired from Simulink simulated feedback control model. Yaw rate setpoint is a two-second sine-ramped step to 10 deg/s starting at $t = 3$ s, a four-second hold, and a two-second sine-ramped step down to 0 deg/s. Roll angle setpoint is a curve of equivalent shape, with magnitude of 10 deg. Sideslip velocity setpoint is constant at 0 m/s.

easily be seen how the wingerons deflect at $t = 3$ s to initiate the positive roll, eliminating the necessity for the boat to be piloted like a bike. In this way, the combination of independent inputs allows us to overcome an inherent behavioral challenge in the original system. We also note that during the turn the front strut is turned to the right and the rear strut is turned left. This is similar to the performance of active four-wheel steering in automobiles and is representative of behavior we expected from the model.

We do note that the magnitude of the wingeron deflection is problematic. The rear foils of the CU hydrofoil boat are only designed to operate from -6° to 13° which is ap-

proximately the extent of the linear region of the lift coefficient slope for the MH115 foils. However, we can see that in order to maintain a moderate 10 deg/s turn, the foils are commanded to deflect up to -20° . When we introduced a saturation block in the Simulink model that gave upper and lower saturation limits to the wingeron deflection, the simulation model showed unstable behavior. This is an effect of the commanded signal not making it to the model due to the saturation block, and the controller therefore being unable to compensate for an effect it is not “aware” of.

CONCLUSIONS & RECOMMENDATIONS

Conclusion

In this paper, we have used theory of aircraft dynamics to expand upon an experimentally-validated state-space model for a single-track hydrofoil boat to include front and rear steering and differential wing control. We mathematically developed a stable feedback control loop for the validated model in a Simulink simulation to prove the efficacy of such an approach and repeated the process for the new multi-input model we developed.

Using the simulation, we demonstrated the feasibility of using multi-input automatic control for the Cedarville University solar boat, and we showed that using all three control inputs available to us will allow the boat to perform excellently while flying on hydrofoils. We believe this work lays an important foundation for the development of an automatic flight control system for Cedarville's solar boat and we hope that future students will be able to make use of this work and realize our dream of returning to compete in the Dutch Solar Challenge.

We further hope that this document can be used as a ground-level reference to anyone interested in multi-input automatic control for the purposes of hydrofoil watercraft, aircraft, or any system otherwise.

Recommendations

While promising, the model presented in this work is not a complete solution in and of itself. As discussed in Section 6.2, the simulation is exceeding the limits for wing deflection. Further work should be performed to overcome this problem.

The model also assumes perfect control of the longitudinal states (e.g forward velocity, pitch, etc.). The model and simulation should either be expanded to account for longitudinal dynamics and include longitudinal control, or be combined and coupled with a separate height and pitch control system to maintain level flight during maneuvers.

Preceding the implementation of the automatic control model on a physical system, we recommend implementing a simulated form of sensor/signal delay and possibly signal noise to test the reactivity and robustness of the control system. For similar reasons, we also suggest experimenting with different sampling rates for the feedback signals.

ACKNOWLEDGEMENTS

The completion of this research could not have been possible without the faculty advisors to the Cedarville University Solar Boat team, Dr. Tim Dewhurst and Dr. Gerry Brown. Thank you for your continued encouragement, wisdom, and support through all the mistakes and learning curves I overcame during this study, and for teaching me how to be an engineer of great character.

Thanks to my friend, classmate, and team member, Daniel Urban, for the countless times you encouraged me in my struggles and for lending an ear as a sounding board for my research and ideas.

Thanks to Dr. Fred Harmon at Cedarville University for helping a mechanical engineering student far out of his depth to understand control theory, and for recommending Dr. Nelson's textbook to me for research.

I am forever thankful to my parents and brother for their love, guidance, and provision through my time in undergrad.

And last but not least, I would like to extend my appreciation to the many not mentioned here who have helped to encourage and motivate me on this journey.

BIOGRAPHY

Jason Paulus is a software auditing and remediation manager in an intern position with Jacobs Engineering Group, working on the Missile Defense Agency's (MDA's) Integrated Research & Development for Enterprise Solutions (IRES) contract. He served as team captain of the Cedarville University Solar Boat team for the 2021 Solar Splash competition in Springfield, OH, and earned his bachelor's degree in Mechanical Engineering from Cedarville University in 2021. Currently residing in Colorado Springs, CO, he enjoys hiking in the beautiful Rocky Mountains.

References

- [1] van Marrewijk, G. P., Schonebaum, J. K., and Schwab, A., 2018. "An experimentally validated dynamical model of a single-track hydrofoil boat". *Naval Engineers Journal*, **130**(1), pp. 113–134.
- [2] Messner, B., and Tilbury, D., 1997. Control tutorials for matlab: state space tutorial. <https://lost-contact.mit.edu/afs/umich.edu/class/ctms/Public/html/matlab42/state/state.htm>. Accessed: 2021-06-28.
- [3] MathWorks. MIMO state-space models. <https://www.mathworks.com/help/control/ug/mimo-state-space-models.html>. Accessed: 2021-06-28.
- [4] Ackermann, J., 1972. "Der entwurf linearer regelungssysteme im zustandsraum". *Automatisierungstechnik*, **20**(12), pp. 297–300.
- [5] MathWorks. Pole placement design. <https://www.mathworks.com/help/control/ref/place.html>. Accessed: 2021-06-28.
- [6] Thompson, E., Jacobson, C., Hopkins, J., Harmon, K., Tanner, C., and Mary, K., 2017. "On the design and manufacturing choices to obtain a stable canard hydrofoil system for a low speed solar boat". Accessed: 2021-06-28.
- [7] Nelson, R. C., 1998. *Flight stability and automatic control*, second ed. McGraw-Hill Education.
- [8] Hintze, J. L., 2007. *NCSS User's Guide III: Regression and Curve Fitting*. NCSS, Kaysville, UT. Accessed: 2021-06-28.